Journal of CO_2 Utilization 34 (2019) 479–489

Contents lists available at ScienceDirect

Journal of CO_2 Utilization

journal homepage: www.elsevier.com/locate/jcou

Supercritical antisolvent particle precipitation and fractionation of rosemary (*Rosmarinus officinalis* L.) extracts

Somaris E. Quintana[a,b,*], David Villanueva-Bermejo[a], Guillermo Reglero[a,c], Mónica R. García-Risco[a], Tiziana Fornari[a]

[a] Institute of Food Science Research (CIAL), CEI UAM + CSIC, Madrid, Spain
[b] Research Group of Complex Fluid Engineering and Food Rheology, University of Cartagena, Cartagena, Colombia
[c] Imdea-Food Institute, CEI UAM + CSIC, 28049 Madrid, Spain

ARTICLE INFO

Keywords:
Supercritical antisolvent precipitation
Rosemary
Antioxidant activity
Morphology
Particle size distribution

ABSTRACT

The simultaneous fractionation and precipitation of an ethanolic extract of rosemary (*Rosmarinus officinalis* L.) using supercritical carbon dioxide anti-solvent technique was studied, with the target of separate in two different fractions the key antioxidants of rosemary (i.e. rosmarinic acid, carnosic acid and carnosol). The effect of pressure and temperature on the fractionation process was investigated, together with the morphology and particle size distribution of the precipitates. Additionally, the chemical composition of the oleoresins were analyzed and reported.

In the range of pressures (9–20 MPa) and temperatures (313–333 K) used in this work, the precipitates presented a 2–3 fold enrichment of rosmarinic acid, while carnosic acid and carnosol were concentrated (2–3 fold enrichment) in the oleoresin fractions. Furthermore, in general, oleoresins presented higher antioxidant activity than precipitates. Particles produced with a nozzle of diameter 101.6 μm were smaller and more spherical with increasing pressure (mean value 4–10 μm at 20 MPa) and decreasing temperature.

1. Introduction

Rosemary (*Rosmarinus officinalis* L.) is a Lamiaceae perennial shrub which grows in many parts of the world [1,2]. It has been cultivated since ancient times and recognized as a natural preservative due to its high antioxidant and antimicrobial activities. These activities are related to the presence of phenolic compound, mainly carnosol, rosmanol, isorosmanol, rosmadiol, carnosic acid, rosmarinic acid, and methyl carnosate [3,4]. Extraction techniques like ultrasound or microwave assisted [5], maceration [6], pressurized liquid extraction [7] or using supercritical carbon dioxide [8,9], are mainly employed to improve the extraction of rosemary antioxidants. Generally, natural extracts are marketed in liquid form, as oily preparations, or in solid form as powders. In general, dried powdered extracts have some advantages over liquid extracts, including lower storage costs and a higher concentration and stability of active substances [10].

Different techniques have been studied and developed to obtain powdered extracts and produce particles such as spray drying, spray chilling, jet milling, spray cooling, lyophilization, liquid antisolvent precipitation, or dry/milling processes [11–14]. However, these methods have several disadvantages, such as a wide particle size distribution (PSD), the possible degradation of the product due to mechanical or thermal stresses, and difficulties in the complete elimination of the organic solvents used in the process [15]. Supercritical Antisolvent (SAS) precipitation is an alternative to these conventional processes and has arisen extensive attention as an environmental-friendly and appropriate way for the production of micro- or nanoparticles of pharmaceutical/bioactive compounds [16–18].

In SAS method, supercritical carbon dioxide ($SCCO_2$) is utilized as an antisolvent. The solute is precipitated from a solution which is expanded through a nozzle while mixed with $SCCO_2$, followed by the nucleation and crystal growth [19]. The morphology and size of the particles are influenced greatly by many factors and their combined effects, such as SAS operating conditions [20–22], solvent type [20], surface tension of the solution [23], fluid dynamics [24–27] and mass transfer [28–32].

Abbreviations: MCP, mixture critical point; PSD, particle size distribution; RE, rosemary ethanolic extract; SAS, supercritical antisolvent precipitation process; $SCCO_2$, supercritical carbon dioxide; SEM, scanning electron microscopy; TEAC, trolox equivalent; TPC, total phenolic compounds

* Corresponding author at: Departamento de Producción y Caracterización de Nuevos Alimentos, Grupo de Investigación Ingredientes Alimentarios Funcionales, Instituto de Investigación en Ciencias de la Alimentación CIAL (CSIC-UAM), CEI UAM + CSIC, Universidad Autónoma de Madrid, 28049 Madrid, Spain.
E-mail address: somaris.quintana@predoc.uam.es (S.E. Quintana).

https://doi.org/10.1016/j.jcou.2019.07.032
Received 1 April 2019; Received in revised form 21 June 2019; Accepted 25 July 2019
Available online 01 August 2019

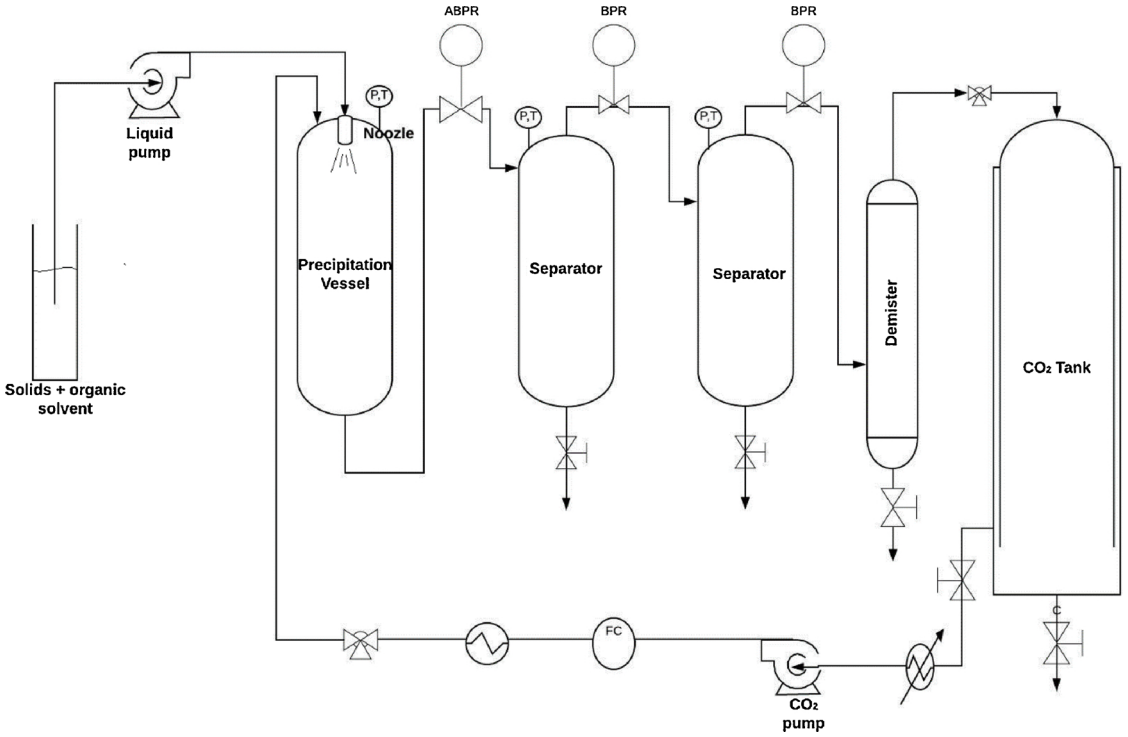

Fig. 1. Schematic diagram of the SAS process. ABPR: Automatic back pressure regulator, BPR: manual back pressure regulator, P: manometer, T: temperature probe, FC: flowmeter.

In general, the precipitation temperature and pressure, the $SCCO_2$ flow, and the concentration of the extract in the solution have significant effect on the size and structure of the particles precipitated during the process [23,33].

Many natural compounds such as carotenoids, quercetin, caffeine, ellagic acid [34], β-carotene [35] or herbal extracts have been precipitated using SAS approach. Likewise, the technique is being used in pharmaceutical products such as ibuprofen or mandelic acid, as well as inorganic materials such as hydrides or polymers (polyethylene glycol or polylactic acid). Also, Matos et al. [36] evaluated the effect of SAS parameters on the co-precipitation of curcumin and poly-vinylpyrrolidone from mixtures of ethanol and acetone, obtaining particle sizes between 96 nm and 135 nm. Franco et al. [37] proposed SAS technique to co-precipitate zein with diclofenac sodium at different operational conditions, gaining a prolonged drug release. SAS precipitation of mango leaf extracts was reported by Guamán-Balcázar et al. [38] obtaining spherical nano- and submicron-particles, with diameters in the range 0.04 – 0.38 μm, and stronger antioxidant activity than the original extracts. Moreover, Widjojokusumo et al. [39] applied SAS to micronizate *Manilkara kauki* L. Dubard's leaf extracts, and Villanueva et al. [40] carried out the fractionation of green tea extracts to obtain decaffeinated fractions with high content of catechins.

Regarding the application of SAS technique to rosemary, Visentin et al. [41] studied the fractionation of an ethanolic oleoresin using a home-made nozzle. They obtained a solid fraction in the precipitation vessel (precipitate) with low yield and concentration of carnosic acid, and a liquid fraction in the separator with high content of this phenolic diterpene (dissolved in ethanol). In addition, Visentin et al. [10] performed the encapsulation of rosemary antioxidants (carnosic and rosmarinic acids) with polymers using SAS precipitation technique at different operating conditions. More recently, Sánchez-Camargo et al. [42] used a pressurized liquid extraction device coupled with an anti-solvent precipitation vessel, with the purpose of determining the bioactivity of the fractions obtained concerning their antiproliferative effect in the HT-29 colon cancer cells. In all these referred works, the SAS fractionation of rosemary antioxidants has been carefully evaluated, but the effect of SAS process conditions on the morphology and particle size distributions of the precipitates has not been considered. In this work, the SAS fractionation of a rosemary ethanolic extract (obtained by ultrasound assisted extraction) to produce a powdered precipitate was studied, considering the effect of process parameters on the recovery of rosemary antioxidants, along with the antioxidant activity and the morphology and particle size distribution of the precipitates.

2. Materials and methods

2.1. Chemicals

CO_2 (99.98% purity) was supplied from Carburos Metálicos (Madrid, Spain). Ethanol (99.5% purity) and Sodium Carbonate anhydrous (99.5% purity) were purchased from Panreac (Barcelona, Spain). Gallic acid standard (> 98% purity), 2,2-Diphenyl-1-pycrilhydrazyl (DPPH, 95% purity), 2,2´-azino-bis (3-ethylbenzothiazoline-6-sulfonic acid) diammonium salt (ABTS, ≥ 95% purity), (±)-6-Hydroxy-2,5,7,8-tetramethyllchromane-2-carboxylic acid (Trolox, 97% purity), Folin-Ciocalteu´s reagent and rosmarinic acid (≥ 98% purity), eucalyptol (≥ 99% purity), linalool (≥ 97% purity), camphor (≥ 95% purity), borneol (≥ 99% purity), 4-terpineol, (+)–terpineol (≥ 99% purity), (1S) - (-) verbenone (≥ 94% purity), -carophyllene Kosher (≥ 80% purity) and carophyllene oxide were purchased from Sigma–Aldrich (St. Louis, MO, USA). Carnosic acid (> 97% purity), purchased from Cymit (Cymit Química S.L., Barcelona, Spain).

2.2. Preparation of rosemary extract

Rosemary (*Romarinus officinalis* L.) leaves harvested in Spain obtained from Murciana herbalist's Murcia Spain) was ground using a Premill 250 hammer mill Lleal S.A. Granollers, Spain). Then, ultrasound assisted extraction (UAE) using an ultrasonic device (Branson Digital Sonifier 550 model Danbury, USA) with an electric power of 200 W and frequency of 60 kHz was accomplished. The extraction was:

carried out with ethanol at 1: 10 (w/v) plant/solvent ratio for 15 min and keeping constant the extraction temperature at 25 °C. The rosemary ethanolic extract (RE) (ethanol + solutes extracted) contained 16.04 mg of solutes in 1 ml of dissolution (1.98% wt). The dissolution was stored at -293.15 K for its use in the SAS process.

2.3. Supercritical antisolvent precipitation

The supercritical antisolvent precipitation was performed using the supercritical technology equipment Thar SF2000 (Thar Technology, PA, USA) (Fig. 1). The equipment comprises two pumps for feeding the supercritical $SCCO_2$ and the liquid solution, respectively, the precipitation vessel and two separators (S1 and S2) each of 500 ml capacity, with independent control of temperature and pressure, coupled with a demister unit. The demister unit is specially designed to separate liquid or solid particles from the outgoing stream, before driving CO_2 to the recycling system and the storage tank. The precipitation vessel consists on a stainless-steel precipitation cell of 273 ml volume where the $SCCO_2$ and liquid solution streams are fed from the top in a co-current manner (coaxial nozzle). The precipitation cell is equipped with a 101.6 μm inner diameter nozzle for the injection of the liquid solution and a porous metallic frit (5 μm in diameter) that is located at the bottom of the precipitator to collect the precipitate.

$SCCO_2$ was pumped into the precipitation vessel until precipitation pressure and temperature conditions were attained. Then, the ethanolic RE was pumped into the precipitator, while maintaining the $SCCO_2$ flow. After 60 min, once the extract fed ends, additional $SCCO_2$ was pumped during 15 min to wash out the residual solvent from the precipitator. During the process, both separators were kept at ambient pressure. The depressurization of the supercritical stream in the separators produced the ethanol precipitation together with those components which did not precipitate into the precipitation vessel (i.e. the components soluble in the $SCCO_2$/ethanol supercritical phase). Finally, the precipitation vessel was depressurized, and the precipitate was collected.

The simultaneous precipitation and fractionation of RE were studied at pressures in the range 8 to 20 MPa, temperatures of 313.15 to 353.15 K, 50 and 60 g/min of $SCCO_2$ flow, and 1.6 g/min of ethanolic RE. The mole fraction of CO_2 in the pseudo-binary supercritical ethanol + CO_2 mixtures ranged from 97.03 to 97.51%. These mole fractions intent to ensure a homogenous phase according to the ethanol + CO_2 binary phase equilibria data reported in the literature [43–45] although at 333.15 K and 8, 9 and 10 MPa these mole fractions are very close to the two-phase gas-liquid boundary. All experiments were carried out feeding the liquid extract for 60 min. The precipitate (solid fraction) was recovered in the frit of the precipitator vessel. The liquid fractions (non-precipitated compounds dissolved in ethanol) were obtained in the two separators. Both liquids were combined, and ethanol was removed by rotary evaporation under vacuum obtaining an oleoresin. Samples were kept at −297.15 K under darkness until analysis.

2.4. Total phenolic compounds and antioxidant activity

The content of total phenolic compounds present in the samples was determined using the Folin-Ciocalteu method [46]. Briefly, 50 μl of extract were mixed with 3 ml of milliQ water and 250 μl of Folin Ciocalteu reagent. The content was thoroughly mixed and after 3 min, 750 μl of sodium carbonate solution (20% mass) and 950 μl of milliQ water were added to the mixture. After 2 h at room temperature in darkness, the absorbance was measured at 760 nm using a Genesys 10S UV–vis spectrophotometer (Thermo Fischer Scientific Inc., MA, USA). The results were expressed as GAE (mg of gallic acid equivalents / g of extract).

The ability of extracts to scavenge DPPH free radicals was determined according to the method described by Brand-Williams et al, [47]. For the reaction, 25 μl of samples were added to 975 μl of DPPH radical in ethanol ($6.1{\cdot}10^{-5}$), which was daily prepared. The reaction took place at room temperature, in the dark, until it reached a plateau. Then, the absorbance was measured at 515 nm in a Genesys 10S UV–vis spectrophotometer (Thermo Fischer scientific, MA, USA). The DPPH concentration in the reaction medium was calculated from a calibration curve determined by linear regression. A control sample, containing the same volume of solvent instead of extract, was used to measure the maximum DPPH absorbance. Trolox was used as reference standard, so results were expressed as TEAC values (μmol Trolox equivalent/g extract). All analyses were done in triplicate.

2.5. HPLC analysis

Carnosol, carnosic and rosmarinic acid were identified and quantified in the samples following the procedures describes by Vicente et al. [48] using a HPLC Prominence-i LC-2030C 3D Plus (Shimadzu) equipped with a RP-C18 (250 × 4.6 mm; 3 μm) chromatography column. The mobile phase consisted of 0.1% of phosphoric acid in water (solvent A) and acetonitrile (solvent B) applying the following gradient: 0–8 min, 77% A, 8–25 min, 25% A, 25–40 min 25% A and the 40–45 min 77% A. Initial conditions were gained in 5 min. The flow rate was constant at 0.7 ml/min. Injection volume was 20 μl and the detection was accomplished using a diode array detection system, storing the signal at a wavelength of 230, 280 and 350 nm.

2.6. GC–MS analysis

Identification and quantification of volatile compounds of samples was carried out by a GS-MS-FID using 7890A system Agilent Technologies Santa Clara, CA, USA) comprising a split/splitess injector FID detector and a mass spectrometer detector 5975C triple-axis. An HP-5MS capillary column (30 m x 0.25 mm i.d. 0.25 μm phase thickness) was used. The chromatographic method starts with an initial temperature of 313.15 K then increased to 423.15 K at 276.15 K/min and was held at 423.15 K for 10 min then from 423.15 to 573.15 K at 279.15 K/min and finally held at 573.15 K for 1 min. Volume of 1 μl of samples was injected in spitless mode. Helium (99.99%) was employed as carrier gas (1 ml/min flow rate). The temperatures were: 523.15 K for injector 503.15 K for the mass spectrometer ion source 553.15 K interface and 423.15 K for quadrupole. The mass spectrometer operated under electron impact mode (70 eV) and it was used in total ion current (TIC) mode and scanned the mass range from 40 to 500 *m/z*.

2.7. Morphology and particle size analysis

Morphologies of particles collected from the precipitation vessel were visually studied by scanning electron microscopy (SEM) with an energy-dispersive X-ray spectrometer (SEM-EDS) XL-30S FEG, Philips (Japan). Samples were placed on carbon tapes and then were coated with a thin chrome layer by a sputter coater. Particle size distributions were measured by light scattering with a laser diffraction system Mastersizer 2000 (Malvern Instruments Ltd., Malvern, UK), equipped with a wet dispersion unit.

3. Results and discussion

3.1. The supercritical antisolvent process

The flow rates of $SCCO_2$ and RE were set in order to reach a percentage of ethanol in CO_2 around 3.2% weight ethanol. It was expected to attain a homogenous CO_2 + ethanol phase at all the different precipitation conditions (pressure and temperature) and thus, ensure the complete elimination of ethanol and produce the precipitation of solid particles [49].

The phase equilibria of the CO_2 + solvent + solute multicomponent

system strongly affect the phenomena taking place in the SAS precipitation process. Different behavior concerning jet mixing and mass transfer were described in the literature, depending on the SAS operational conditions, which can be located below the mixture critical point (MCP), near above the MCP or far above the MCP [25]. Furthermore, fluid dynamics and mass transfer determine the production of precipitates, and the complexities of these mechanisms are responsible for the great variety of particle size and morphology generally obtained.

When the operational conditions of SAS process are below the MCP (subcritical conditions) small droplets of the solvent (containing the solute) are produced as a result of the jet break-up. The surface tension persists and a multiphase gas-liquid-solid mixing system results. The mass transfer of CO_2 into the droplets (solvent-rich phase) together with the solvent evaporation into the CO_2-rich phase lead to the supersaturation of the solute and produce its precipitation. That is, the formation of particles is induced by the $SCCO_2$ antisolvent effect and by the organic solvent depletion in the droplets formed by the nozzle. Consequently, in the case of SAS subcritical gaseous conditions, microparticles and expanded microparticles (hollow core particles) with regular forms are obtained. Nevertheless, if the SAS subcritical conditions are located within the gas-liquid region, irregular particles and agglomeration due to residual solvent generally occur.

On the other hand, for SAS operational conditions far above the MCP, the mixing of CO_2 with the solvent is produced instantaneously since the surface tension vanishes before an appreciated jet break-up is obtained and thus, no liquid-gas interphase occurs. It was generally stated [49] that smaller particles (nanoparticles) are obtained at pressures relatively larger than those corresponding to the MCP, produced by their condensation from a gaseous phase. Yet, for conditions near above the MCP the behavior size and morphology depend on the time that it takes to vanish the surface tension and the time of jet break-up. In general, spherical microparticles were observed when SAS process was performed in the proximity of the MCP.

In the present studyas stated before,not all the solutes of RE precipitate in the precipitation chamber since some of them are soluble in the supercritical CO_2 + ethanol phase. In this way two different fractions were obtained from the RE a powder in the precipitation vessel (: P: precipitate) and a viscous fraction (: O: oleoresin) which was recovered from the separators after evaporation of ethanol.

The SAS experimental assays carried out in this work, together with the corresponding yield (Y), total phenolic compound (TPC) and antioxidant capacity (TEAC values) of the fractions obtained (P and O) are shown in Table 1.

First, supercritical antisolvent precipitation was carried out by duplicate at the selected conditions 20 MPa, 313.15 K and 50 g/min of $SCCO_2$ flow rate (Exp. 10 and 11 in Table 1) to assess the reproducibility of the method. Regarding precipitation yield (mass of extract precipitated / mass of extract feed) the values obtained were 44.74 and 45.07%, respectively, and the oleoresin yields (mass of extract recovered in the separators / mass of extract feed) were 43.03 and 43.64%, respectively, for Exp. 10 and 11. These results indicate a mean deviation of 0.23 and 0.43, respectively, for P and O yields, and a total recovery of the mass feed larger than 87%. Further analysis of the precipitates obtained in Exp. 10 and 11 confirmed low mean deviation in the rosmarinic acid, carnosol and carnosic acid content (Table 2), so as total phenolic content and TEAC value (Table 1) and mean size of particle (Table 4).

Table 2
Mass fraction of main rosemary antioxidants (rosmarinic acid, carnosol and carnosic acid) determined in the precipitates and oleoresins by HPLC analysis. C: mass fraction, E: enrichment factor.

Exp.	antioxidant compound	Precipitate (P)		Oleoresin (O)	
		C / mg/g	E	C /mg/g	E
1	Rosmarinic acid	45.40	2.79	12.20	0.74
	Carnosol	4.80	0.33	19.40	1.33
	Carnosic acid	24.50	0.24	123.20	1.20
2	Rosmarinic acid	21.60	1.33	7.00	0.43
	Carnosol	13.90	0.95	19.40	1.33
	Carnosic acid	79.00	0.77	172.50	1.68
3	Rosmarinic acid	21.60	1.65	3.60	0.22
	Carnosol	13.40	0.92	24.00	1.64
	Carnosic acid	77.80	0.76	224.60	2.18
4	Rosmarinic acid	19.80	1.51	1.40	0.09
	Carnosol	13.40	0.92	35.70	2.45
	Carnosic acid	76.20	0.74	172.50	1.68
5	Rosmarinic acid	24.80	1.89	1.80	0.11
	Carnosol	2.00	0.14	40.40	2.77
	Carnosic acid	13.40	0.13	299.20	2.91
6	Rosmarinic acid	24.60	1.88	1.20	0.07
	Carnosol	2.00	0.14	21.20	1.45
	Carnosic acid	13.20	0.13	132.20	1.29
7	Rosmarinic acid	20.00	1.23	2.80	0.17
	Carnosol	13.80	0.95	15.50	1.06
	Carnosic acid	81.40	0.79	138.80	1.35
8	Rosmarinic acid	25.50	1.56	1.40	0.09
	Carnosol	3.00	0.21	39.60	2.71
	Carnosic acid	16.20	0.16	299.20	2.91
9	Rosmarinic acid	32.20	1.98	0.00	0.00
	Carnosol	0.80	0.05	30.20	2.07
	Carnosic acid	5.80	0.06	233.80	2.27
10	Rosmarinic acid	39.40	2.42	2.80	0.17
	Carnosol	1.00	0.07	29.90	2.05
	Carnosic acid	9.60	0.09	228.20	2.22
11	Rosmarinic acid	38.00	2.33	2.80	0.17
	Carnosol	0.80	0.05	29.90	2.05
	Carnosic acid	7.40	0.07	226.20	2.20

Table 1
Yield (Y) expressed as mass recovered of precipitate or oleoresin/mass of extract feed, Total Phenolic Content (TPC) expressed as GAE (mg of gallic acid equivalents/g) and antioxidant activity expressed as TEAC value (μMol Trolox equivalent/g).

Precipitation conditions				Precipitate (P)			Oleoresin (O)		
Exp.	P / MPa	T / K	CO_2 flow / g/min	Y %	TPC mg GAE/g	TEAC μMol Trolox equivalent/g	Y %	TPC mg GAE/g	TEAC μMol Trolox equivalent/g
1	8	333.15	60	8.43	222.98 ± 0.32	975.42 ± 3.06	56.28	137.42 ± 0.01	760.89 ± 1.34
2	9	333.15	60	39.36	148.91 ± 0.32	756.23 ± 0.35	11.49	145.12 ± 0.01	850.63 ± 7.69
3	10	333.15	60	46.84	138.54 ± 2.05	523.47 ± 3.06	16.60	137.64 ± 0.47	895.93 ± 6.88
4	10	333.15	50	68.10	136.53 ± 1.10	454.19 ± 0.60	18.82	155.60 ± 4.73	1066.85 ± 2.41
5	10	313.15	60	53.82	103.84 ± 0.01	448.44 ± 2.88	38.10	162.52 ± 0.01	1160.23 ± 1.29
6	10	313.15	50	57.63	107.41 ± 0.95	449.06 ± 2.95	36.48	159.62 ± 0.95	1187.27 ± 7.96
7	10	353.15	60	41.16	138.76 ± 1.10	749.57 ± 1.67	7.29	119.21 ± 0.21	663.91 ± 2.06
8	15	333.15	60	59.17	115.11 ± 0.16	456.97 ± 1.33	32.32	121.47 ± 0.32	1344.52 ± 0.69
9	20	333.15	60	42.84	123.37 ± 0.47	500.62 ± 0.39	38.16	147.79 ± 2.52	1291.76 ± 5.95
10	20	313.15	50	44.74	177.35 ± 2.91	557.00 ± 0.01	43.03	218.08 ± 9.72	1356.65 ± 0.01
11	20	313.15	50	45.07	175.44 ± 6.70	561.43 ± 0.03	43.64	221.68 ± 6.70	1376.87 ± 0.06

3.2. Effect of pressure, temperature and $SCCO_2$ flow on precipitation yield

The effect of temperature on the fractionation and precipitation of RE was studied at 10 MPa, 50–60 g/min of $SCCO_2$ and varying temperature in the range of 313.15 to 353.15 K (Exp. 3, 4, 5, 6, and 7 in Table 1). Additionally, the effect of pressure was investigated keeping temperature constant at 333.15 K, $SCCO_2$ flow at 60 g/min, and varying pressure from 8 to 20 MPa (Exp. 1, 2, 8 and 9 in Table 1). The flow rate of the RE was set to 1.6 g/min in all cases.

Considering both the mass of precipitate (P) and the mass of oleoresin (O) recovered in the separators48 to 94% of the total mass of solids fed to the SAS process was recovered. The major losses of solids pumped were produced at the higher temperature 353 K Exp. 7) and at lower precipitation pressures (Exp. 1 and 2). In general yields in the precipitation chamber were higher than oleoresin yields. This result is in accordance with previous results obtained by Sánchez-Camargo et al. [42] in the SAS precipitation of an : ethanol: water rosemary extract obtained by pressurized liquid extraction. Nevertheless a distinct behavior at 8 MPa and 313 K (Exp. 1) was observed with extremely low precipitation yield in comparison with the rest of experiments. At these pressure and temperature conditions the CO_2 + ethanol mixture is very close to the vapor-liquid equilibrium state [4344] and thus it is presumed that some small drops formed by the nozzle were dragged out of the precipitation chamber and precipitation was drastically reduced. The increase of pressure from 9 to 15 MPa at constant temperature (333 K) and $SCCO_2$ flow (60 g/min) produced a linear increase of both P and O yields (R^2 values of 0.95 and 0.99 respectively improving the total mass of RE recovered from 50.85% at 9 MPa to 91.49% at 15 MPa. Yet further increase of pressure to 20 MPa seem not to improve precipitation yield and/or total extract recovery.

The opposite behavior was observed concerning the effect of temperature on P and O yields. That is, increasing temperature at constant pressure (10 MPa) and $SCCCO_2$ flow (60 g/min) a linear decrease of both P and O yields (R^2 values of 0.99 and 0.95, respectively) was observed, decreasing the total mass of RE recovered from 53.82% at 313 K to 41.16% at 353 K. Regarding the effect of the $SCCO_2$ flow on process yields, despite the narrow range of values studied in this work, a decrease of precipitation yield was observed when $SCCO_2$ flow increased form 50 and 60 g/min (Exp. 3 and 4 at 333 K, and 5 and 6 at 313 K). Both the increase of temperature and the increase of CO_2 flow suppose a higher dragging of volatile compounds with the CO_2 stream and thus, lower amounts of solutes were recovered with increasing temperature and CO_2 flow.

3.3. Phenolic compounds and antioxidant activity of precipitates and oleoresins

Table 1 shows the amount of Total Phenolic Compounds (TPC) expressed as mg GAE/g in the samples obtained (P and O) at the different experimental conditions, along with their antioxidant capacity expressed as TEAC value (μmol Trolox equivalent/g extract).

In general, samples with high TPC values present also high antioxidant activity (high TEAC values). This result is in general accordance with the literature [50]. For the precipitates (P), the TPC are between 103.84 and 177.35 mg GAE/g and the TEAC values ranged from 448.44 to 756.23 μMol Trolox equivalent/g. The TPC values of oleoresins (O) ranged from 119.91 to 218.08 mg GAE/g and TEAC values were in the range 663.91–1356 μMol Trolox equivalent/g. Although differences in the TPC content of samples P and O obtained in a particular experiment were not very large, in general, the antioxidant activity of the oleoresin is considerably higher than that of the precipitate (Fig. 2). Taking into account the TPC content and TEAC value of the RE (121.58 mg GAE/g and 661.84 ± 0.25 μmol Trolox equivalent/g, respectively) is mainly highlighted the potential enrichment of TPC and improvement of antioxidant activity achieved by means of the supercritical fractionation.

The effect of pressure on the content of phenolic compounds and the antioxidant activity is depicted in Fig. 3. Phenolic compounds are substances with recognized antioxidant activity [51,52] and thus, the higher the TPC the higher the antioxidant activity (higher TEAC values). TPC values and TEAC values decrease with increasing pressure in the precipitation chamber, denoting a relation among polyphenols content and antioxidant activity. Nevertheless, in the case of the oleoresins, TEAC values increase with pressure although TPC slightly varied. The opposite is observed concerning the effect of temperature (Fig. 4) since the increase of temperature produce increasing values of both TPC and TEAC in precipitates while decreasing values in the oleoresins. Minor influence of the $SCCO_2$ flow on the TPC and TEAC values were observed, probably due to the narrow range of values explored (Exp. 3 and 4; Exp. 5 and 6).

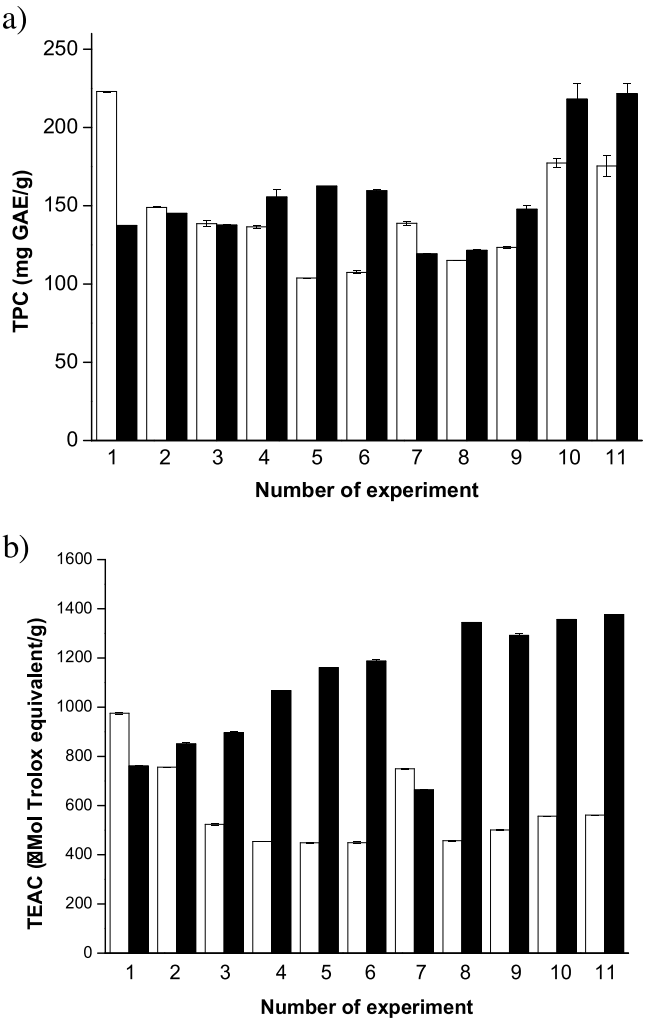

Fig. 2. (a) Content of total phenolic compounds (TPC values) and (b) antioxidant activity (TEAC values) obtained in (□) precipitates and (■) oleoresins.

Then, as a general trend, it can be concluded that the precipitates with the higher antioxidant activity were obtained at the lower pressures and higher temperatures, while the opposite resulted in the case of oleoresins. This general trend can be explained in terms of the TPC of precipitates and oleoresins, since higher amounts of TPC were determined for the precipitates at lower pressures and higher temperatures and the opposite resulted in the case of oleoresins (Figs. 3 and 4).

3.4. Fractionation of rosmarinic acid, carnosic acid and carnosol

Table 2 shows the results of the quantification of the main and well-known rosemary antioxidants, e.g. rosmarinic acid, carnosic acid and carnosol, in precipitates and oleoresin. The varied conditions applied in

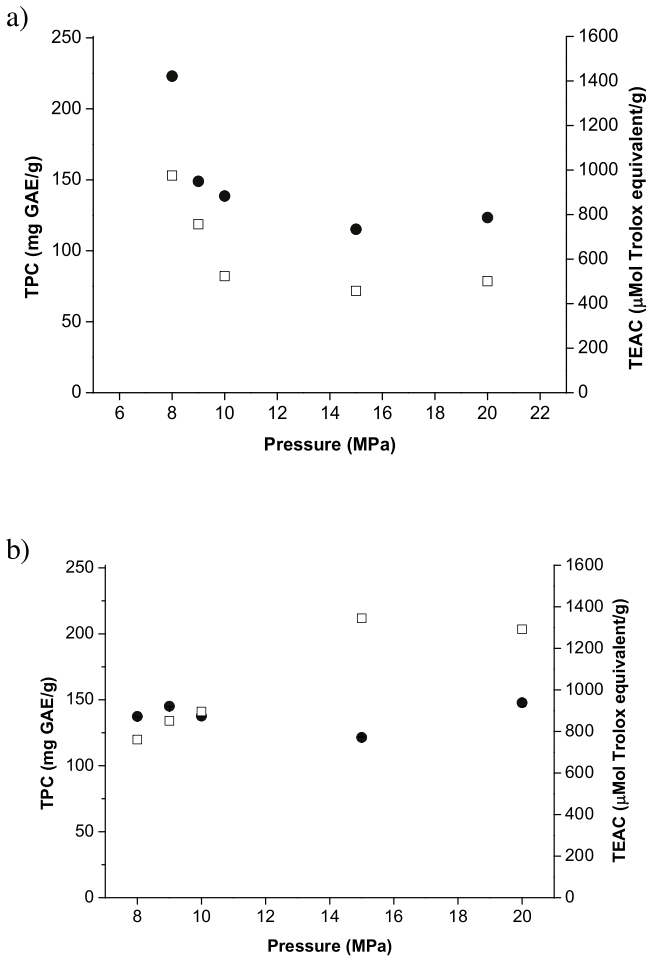

Fig. 3. Effect of pressure on (●) TPC and (□) TEAC values in (a) precipitates and (b) oleoresins. T = 333.15 K; CO_2 flow = 60 g/min.

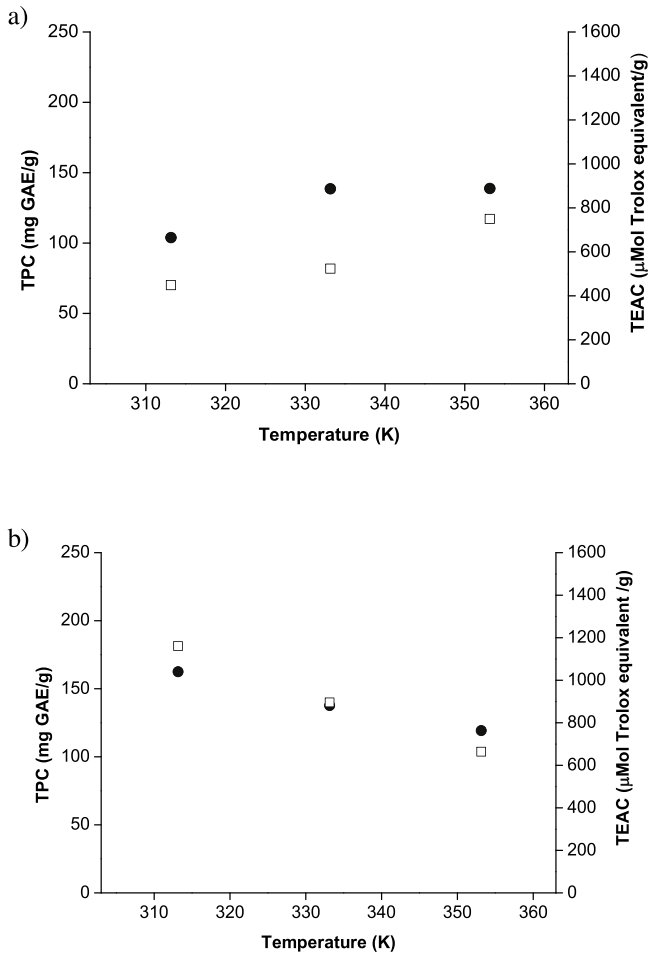

Fig. 4. Effect of temperature on (●) TPC and (□) TEAC values in (a) precipitates and (b) oleoresins. P = 10 MPa; CO_2 flow = 60 g/min.

the SAS precipitation process resulted in a different fractionation of these rosemary antioxidant compounds.

In general, the precipitate presented higher concentrations of rosmarinic acid in comparison with the oleoresin. On the contrary, higher concentrations of carnosic acid and carnosol were obtained in the oleoresins. This behavior was expected taking into account the solubility of these compounds in a supercritical phase comprising $SCCO_2$ and ethanol acting as a cosolvent. According with the literature, while rosmarinic acid is almost no soluble in $SCCO_2$, carnosic acid exhibits solubilities up to 0.4 mg/g [53,54]. Thus, rosmarinic acid is mainly recovered in the precipitation vessel while carnosic acid (dissolved in the supercritical stream which flows out of the precipitation vessel) is recovered in the separators.

Fig. 5 shows the recovery of rosmarinic acid, carnosic acid and carnosol (mg compound/100 g of RE) at 333.15 K and different pressures (9–20 MPa) obtained in precipitates and oleoresins. In the range of pressures explored, rosmarinic acid recovery (Fig. 5(a)) was significantly higher in the precipitates, increased with pressure and attained a maximum at 15 MPa. Regarding carnosic acid and carnosol (Fig. 5(b) and (c)) the higher recoveries were obtained in the separators (oleoresin product) and as in the case of rosmarinic acid a maximum recovery was observed at 15 MPa.

Moreover, in comparison with the RE (14.6 mg/g of rosmarinic acid, 102.8 mg/g of carnosic acid and 16.4 of carnosol) a rosmarinic acid enrichment of 1.33–2.79 was produced in the precipitates while 1.20–2.91 carnosic acid enrichment and 1.06–2.77 carnosol enrichment were obtained in the oleoresins. Thus, using SAS technique, a selective fractionation of these compounds was attained.

3.5. Oleoresin composition

Table 3 shows the components of rosemary essential oil identified and quantified in the oleoresins by GC–MS analysis. These compounds were not identified or identified in very small amounts in the precipitates (data not shown). Table 3 also includes the mass fraction of main rosemary antioxidants (rosmarinic acid, carnosic acid and carnosol) determined in the oleoresins by HPLC.

According with the literature, the main compounds of rosemary essential oil are eucalyptol, camphor and borneol. The rosemary oleoresins produced in this work contain large amounts of camphor (30–198 mg/g), eucalyptol (25–65 mg/g) and borneol (10–70 mg/g), being the most abundant compounds identified by GC–MS. Considering the compounds identified by GC–MS together with those determined by HPLC, the total amount of oleoresin quantified varies from 23.4 to 60.9%.

3.6. Analysis of morphology and particle size of precipitates

3.6.1. Particle morphology

Scanning electron micrograph (SEM) of the RE and the precipitates (P) are shown in Fig. 6. The image corresponding to RE (Fig. 6(a)) showed that the powder is mostly non-equiaxed and angular in morphology.

The shape of the precipitated particles showed micronized size with different characteristics depending on SAS pressure. At 313.15 K, 9 and 10 MPa (Fig. 6(b) and (c)) the particles are thin, elongated, with the form of fibers and agglomerates of particles are observed showing

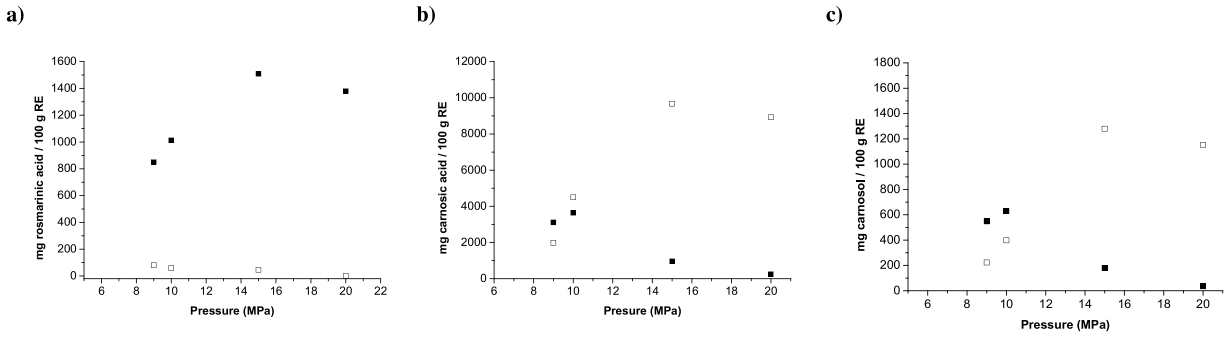

Fig. 5. Recovery of (a) rosmarinic acid, (b) carnosic acid and (c) carnosol (mg/100 g of RE) at 333.15 K and different pressures (9–20 MPa) obtained in precipitates (■) and oleoresins (□).

Table 3
Composition of the oleoresins obtained in the supercritical anti-solvent fractionation of rosemary extract. The values are expressed as mg/g.

Exp	1	2	3	4	5	6	7	8	9	10	11
P (MPa)	8	9	10	10	10	10	10	15	20	20	20
T (K)	333.15	333.15	333.15	333.15	313.15	313.15	353.15	333.15	333.15	313.15	313.15
CO_2 flow (g/min)	60	60	60	50	60	50	60	60	60	50	50
GC-MS											
(-)-4-terpineol	1.97	6.68	6.04	4.52	2.14	2.52	9.38	4.65	0.98	1.43	1.67
camphor	29.44	133.38	153.28	111.02	51.80	54.63	198.99	54.05	64.69	34.21	34.04
alpha terpineol	4.06	28.88	22.82	19.16	10.24	11.07	40.12	11.28	3.29	7.55	7.26
borneol	9.84	50.44	47.13	35.57	17.66	19.03	71.70	15.46	9.38	9.48	9.75
caropyllene	3.00	19.81	20.38	7.63	4.58	5.06	10.33	5.94	2.43	4.12	4.30
eucalyptol	25.31	31.90	65.60	48.39	25.83	26.78	58.34	31.56	28.68	24.23	25.04
verbenone	5.78	22.50	22.57	14.83	6.18	6.58	30.16	13.68	8.35	3.86	3.86
alpha carophyllene	n.i.	8.31	4.54	n.i.	6.10	n.i.	n.i.	1.86	n.i.	n.i.	n.i.
linalool	n.i.	3.61	6.81	3.18	0.87	1.21	7.05	1.78	1.97	u.q.l	u.q.l
carophyllene oxyde	n.i.	13.52	7.60	8.79	n.i.	6.28	16.23	4.15	n.i.	n.i.	n.i.
HPLC											
rosmarinic acid	12.20	7.00	3.60	1.40	1.80	1.20	2.80	1.40	0.00	2.80	2.60
carnosol	19.40	19.40	24.00	35.70	40.40	21.20	15.50	39.60	30.20	31.20	30.40
carnosic acid	123.20	172.50	224.60	172.50	299.20	132.20	138.80	299.20	233.80	231.20	223.20
% mass quantified	23.4	51.8	60.9	46.3	46.7	28. 8	60.0	48.5	38.4	35.0	34.2

n.i.: non identified.
u.q.l.: under quantification limit (< 0.02 mg/ml).

Table 4
Mean particle size of SAS particles in the precipitates.

Exp.	P /MPa	T / K	CO_2 flow / g/ min	d (0.1) μm	d (0.5) μm	d (0.9) μm
1	8	333.15	60	3.12	21.08	45.98
2	9	333.15	60	5.37	20.32	40.60
3	10	333.15	60	4.22	18.15	42.14
4	10	333.15	50	6.39	15.49	30.21
5	10	313.15	60	3.40	10.17	22.58
6	10	313.15	50	3.77	9.81	20.64
7	10	353.15	60	6.96	31.89	66.29
8	15	333.15	60	0.27	3.43	8.97
9	20	333.15	60	0.16	0.62	9.77
10	20	313.15	50	0.28	1.16	5.28
11	20	313.15	50	0.24	1.52	4.15

varying sizes. When the pressure increased to 15 and 20 MPa (Fig. 6(d) and (e)) the particles tend to be smaller (< 1 μm) and more spherical. Similar results were reported by Villanueva-Bermejo et al., [55] concerning the precipitation of *Achilea millefolium* L. ethanolic extract, where more irregular morphologies were found in the precipitates obtained at 10 MPa in comparison to those obtained at 20 MPa. Also, Guamán-Balcázar et al. [38] found spherical and small particles in the precipitation of a mango leaf extracts using pressures over 15 MPa.

Certainly, the size and morphology of the particles depends on the type of solutes, but as mentioned before also depend on the operating conditions, particularly concerning the location of SAS operational conditions with respect to the MCP. The phase equilibria data of the multicomponent CO_2 + ethanol + RE system is not available in the literature (and difficult to attain), but some analysis and conclusions can be established considering the MCP of the CO_2 + ethanol binary mixture. Nevertheless, it has to be highlighted that in the case of solutes with high solubility in the CO_2 + ethanol phase, as is the case of some RE solutes, the MCP of the multicomponent mixture can be rather different from that of the binary CO_2 + ethanol MCP [25].

According to the phase equilibria data reported in the literature [43–45] the MCP of the binary CO_2 + ethanol at 313.15, 333.15 and 353.15 K are, respectively, 8.2, 10.6 and 15.0 MPa. Thus, considering these data, the operating conditions of experiments 5, 6 and 8–11 are clearly above the MCP, while the rest of experiments are very close or below of the MCP. Consequently, at 333.15 K and the lower pressures (Exp. 2 and 3) irregular forms and agglomerates of different size were observed, probably due to operating subcritical conditions located within the gas-liquid region. When pressure is increased (Exp. 8 and 9) and thus the SAS conditions are above the MCP, spherical and regular microparticles were obtained (Fig. 6).

The effect of temperature at constant pressure (10 MPa) on the particle's morphology showed more regular spherical structures in the precipitates at the lower temperature (313.15 K) since at this temperature the experimental SAS conditions are far above the MPC (Exp. 5 and 6). Increasing temperature at 10 MPa, particles tend to present more irregular forms including filament pieces, conglomerates and spheres (imagens not shown) due to subcritical and most probably two-phase operational conditions.

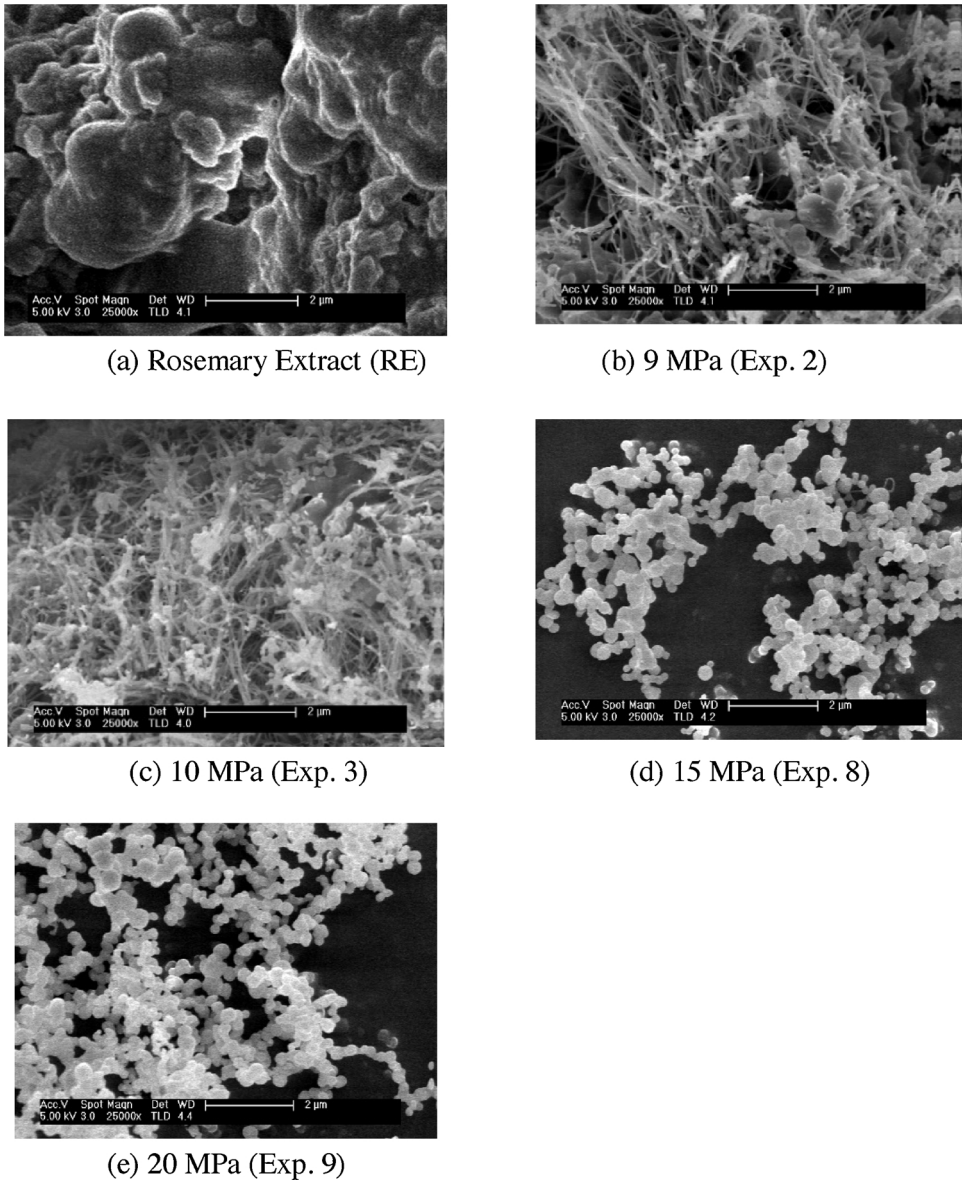

Fig. 6. SEM images (25000x) of rosemary extract (RE) and SAS precipitates (P) at 333.15 K and 60 g/min and different pressures.

3.6.2. Particle size

As mentioned before, it is generally recognized that smaller particles (nanoparticles) are obtained at pressures relatively larger than those corresponding to the MCP [22]. Nevertheless, some authors have reported the opposite effect [55].

The particle size distribution and the most significant statistical variables obtained in this work are shown in Fig. 7 and Table 4. The size of the precipitates is in the range of 0.62–21.06 µm. As expected, all samples presented particle sizes lower than the RE. Smaller particles were successfully achieved by increasing the precipitation pressure, i.e. the mean diameter of particles obtained at 9 MPa (Exp. 2) was 20.31 µm while at 15 MPa (Exp. 8) was 5.39 µm.

With respect to the effect of pressure on particle size, Fig. 7 shows the particle size distribution of the RE and the SAS precipitates at 333.15 K, 60 g/min of CO_2 flow and different precipitation pressures. The distributions are moderately narrow, normal and in appearance bimodal for RE and for the precipitates obtained at 9 and 10 MPa (Exp. 2 and 3). When the precipitation pressure increases to 15 and 20 MPa (Exp 8 and 9) the behavior appears as a multi-modal distribution, with significant smaller sizes. Furthermore, the CO_2 flow did not influence particle size in the range of flow rates explored, and regarding temperature (Exp. 3, 5 and 7) it was observed a decrease of particle size with a decrease of temperature (Table 4).

The particle size distribution obtained can be explained in terms of the SAS operational conditions in relation to the MCP [25]. Conditions far above the MCP resulted in smaller particles as can be observed in Table 4 for Exp. 5, 6 and 8–11, being the smaller particles at the higher pressures.

4. Conclusion

Supercritical anti-solvent SAS precipitation of an ethanolic RE permits the simultaneous fractionation and precipitation of two rosemary fractions: a dry powder with small aggregate particles of irregular shape and an oleoresin resulted after ethanol removal.

A selective separation of the main rosemary antioxidants was observed in the range of conditions studied. In comparison with the RE, a 2-fold increase of the rosmarinic acid mass fraction was obtained in the precipitates at 15–20 MPa and 313 K, while a 2-fold increase of the mass fraction of carnosic acid and carnosol in the corresponding oleoresin. Furthermore, particles with smaller size and more spherical shape were obtained with increasing pressure and decreasing

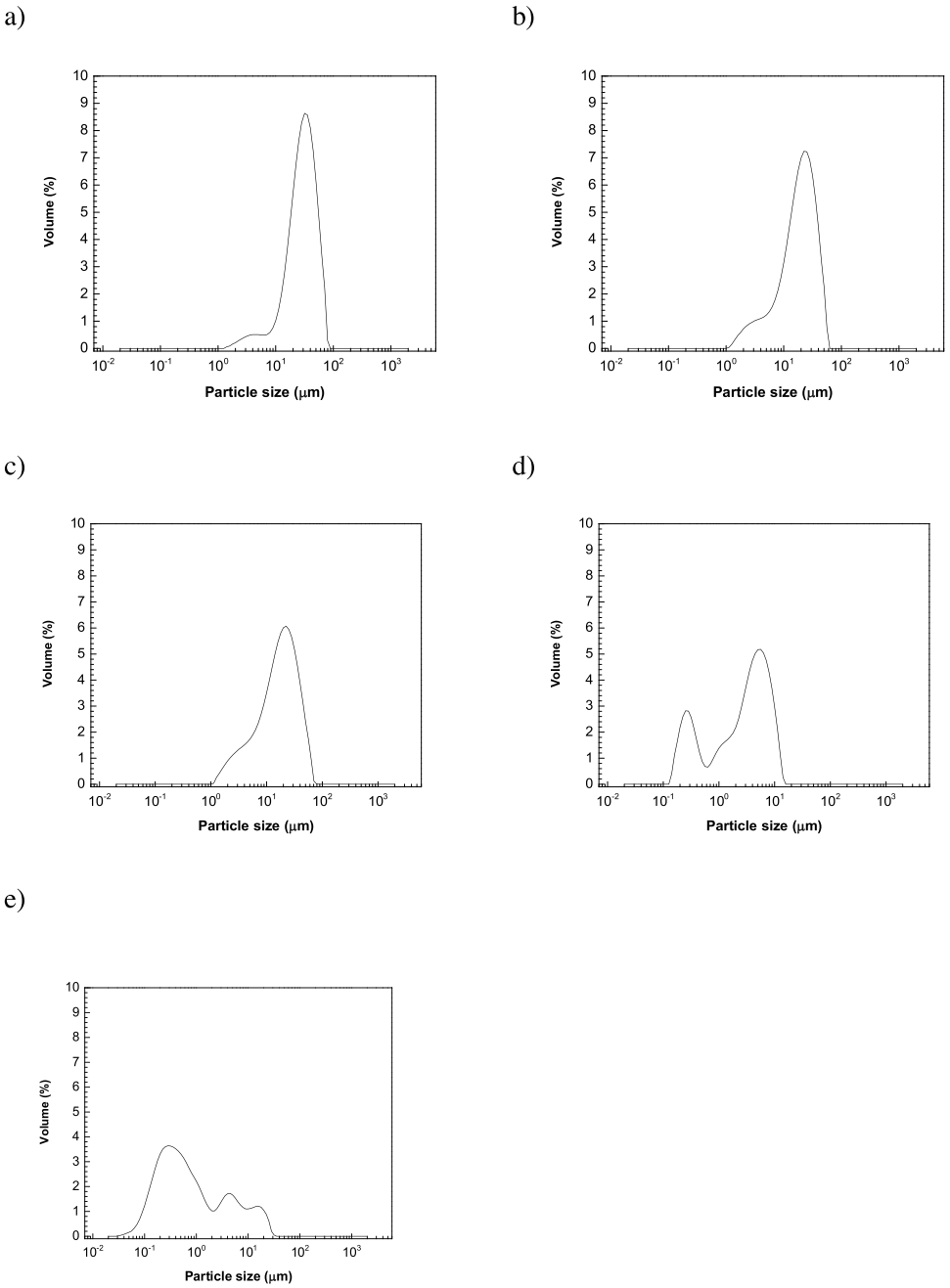

Fig. 7. Particle size distribution of (a) RE and precipitates at 333.15 K, 60 g/min of CO_2 flow and different pressures: (b) 9 MPa, (c) 10 MPa, (d) 15 MPa and (e) 20 MPa.

temperature. Thus, the smaller particle size and more homogeneous particle size distribution were obtained at 313 K and 15–20 MPa, which are SAS operational conditions far above the mixture critical point.

Considering the selective effect of SAS precipitation to separate rosemary antioxidants, it can be concluded the utility of this technique to produce high valued bioactive ingredients with potential application in food products or nutraceuticals. Further studies are under development to determine the anti-inflammatory activity of precipitates and oleoresins in comparison with the initial rosemary extract.

Declaration of Competing Interest

The authors declare that they have no known competing financial interests or personal relationships that could have appeared to influence the work reported in this paper.

Acknowledgements

The authors gratefully acknowledge the financial support from Ministerio de Economía y Competitividad of Spain (Proyect AGL2016-76736-C3-1-R). Somaris E. Quintana is grateful for the funding provided by Gobernación de Bolivar and Fundación Ceiba, Colombia, in the project “Bolívar Gana con Ciencia”.

References

[1] M.R. Ai-Sereiti’, M. Abu-Amer, P. Sen, Pharmacology of Rosemary (*Rosmarinus Oificinalis* Linn.) and its Therapeutic Potentials, (1999).

[2] A. Porte, R.L. de, O. Godoy, D. Lopes, M. Koketsu, S.L. Gonçalves, H.S. Torquilho, Essential oil of *Rosmarinus officinalis* L. (Rosemary) from Rio de Janeiro, Brazil, J. Essent. Oil Res. 12 (2000) 577–580, https://doi.org/10.1080/10412905.2000.9712163.

[3] E. Ibañez, A. Kubátová, F.J. Señoráns, S. Cavero, G. Reglero, S.B. Hawthorne, Subcritical Water Extraction of Antioxidant Compounds from Rosemary Plants, (2002), https://doi.org/10.1021/JF025878J.

[4] H.J. Damien Dorman, S.G. Deans, R.C. Noble, P. Surai, Evaluation in vitro of plant essential oils as natural antioxidants, J. Essent. Oil Res. 7 (1995) 645–651, https://doi.org/10.1080/10412905.1995.9700520.

[5] S. Rodríguez-Rojo, A. Visentin, D. Maestri, M.J. Cocero, Assisted extraction of rosemary antioxidants with green solvents, J. Food Eng. 109 (2012) 98–103, https://doi.org/10.1016/J.JFOODENG.2011.09.029.

[6] G. De, A.R. Oliveira, A.E. De Oliveira, E.C. Da Conceição, M.I.G. Leles, Multiresponse optimization of an extraction procedure of carnosol and rosmarinic and carnosic acids from rosemary, Food Chem. 211 (2016) 465–473, https://doi.org/10.1016/j.foodchem.2016.05.042.

[7] M. Herrero, M. Plaza, A. Cifuentes, E. Ibáñez, Green processes for the extraction of bioactives from rosemary: chemical and functional characterization via ultra-performance liquid chromatography-tandem mass spectrometry and in-vitro assays, J. Chromatogr. A. 1217 (2010) 2512–2520, https://doi.org/10.1016/J.CHROMA.2009.11.032.

[8] G. Vicente, S. Molina, M. González-Vallinas, M.R. García-Risco, T. Fornari, G. Reglero, A.R. de Molina, Supercritical rosemary extracts, their antioxidant activity and effect on hepatic tumor progression, J. Supercrit. Fluids 79 (2013) 101–108, https://doi.org/10.1016/J.SUPFLU.2012.07.006.

[9] G. Vicente, D. Martín, M.R. García-Risco, T. Fornari, G. Reglero, Supercritical carbon dioxide extraction of antioxidants from rosemary (*Rosmarinus officinalis*) leaves for use in edible vegetable oils, Oils Fats 61 (2002) 689–697.

[10] A. Visentin, S. Rodríguez-Rojo, A. Navarrete, D. Maestri, M.J. Cocero, Precipitation and encapsulation of rosemary antioxidants by supercritical antisolvent process, J. Food Eng. 109 (2012) 9–15, https://doi.org/10.1016/j.jfoodeng.2011.10.015.

[11] E. Esposito, R. Roncarati, R. Cortesi, F. Cervellati, C. Nastruzzi, Production of eudragit microparticles by spray-drying technique: influence of experimental parameters on morphological and dimensional characteristics, Pharm. Dev. Technol. 5 (2000) 267–278, https://doi.org/10.1081/PDT-100100541.

[12] H.-J. Lee, J.-H. Kang, H.-G. Lee, D.-W. Kim, Y.-S. Rhee, J.-Y. Kim, E.-S. Park, C.-W. Park, Preparation and physicochemical characterization of spray-dried and jet-milled microparticles containing bosentan hydrate for dry powder inhalation aerosols, drug Des, Devel. Ther. Volume 10 (2016) 4017–4030, https://doi.org/10.2147/DDDT.S120356.

[13] T. Morita, Y. Horikiri, T. Suzuki, H. Yoshino, Preparation of gelatin microparticles by co-lyophilization with poly(ethylene glycol): characterization and application to entrapment into biodegradable microspheres, Int. J. Pharm. 219 (2001) 127–137, https://doi.org/10.1016/S0378-5173(01)00642-1.

[14] X. Chang, J. Bao, G. Shan, Y. Bao, P. Pan, Crystallization-driven formation of diversified assemblies for supramolecular poly(lactic acid)s in solution, Cryst. Growth Des. 17 (2017) 2498–2506, https://doi.org/10.1021/acs.cgd.7b00013.

[15] W. Wang, G. Liu, J. Wu, Y. Jiang, Co-precipitation of 10-hydroxycamptothecin and poly (l-lactic acid) by supercritical CO2 anti-solvent process using dichloromethane/ethanol co-solvent, J. Supercrit. Fluids 74 (2013) 137–144, https://doi.org/10.1016/J.SUPFLU.2012.11.022.

[16] P. Girotra, S.K. Singh, K. Nagpal, Supercritical fluid technology: a promising approach in pharmaceutical research, Pharm. Dev. Technol. 18 (2013) 22–38, https://doi.org/10.3109/10837450.2012.726998.

[17] P.B. Deshpande, G.A. Kumar, A.R. Kumar, G.V. Shavi, A. Karthik, M.S. Reddy, N. Udupa, Supercritical fluid technology: concepts and pharmaceutical applications, PDA J. Pharm. Sci. Technol. 65 (2011) 333–344, https://doi.org/10.5731/pdajpst.2011.00717.

[18] M. Sarkari, I. Darrat, B.L. Knutson, Generation of microparticles using CO_2 and CO2-philic antisolvents, AIChE J. 46 (2000) 1850–1859, https://doi.org/10.1002/aic.690460913.

[19] A. Tabernero, E.M. Martín del Valle, M.A. Galán, Supercritical fluids for pharmaceutical particle engineering: methods, basic fundamentals and modelling, Chem. Eng. Process. Process Intensif. 60 (2012) 9–25, https://doi.org/10.1016/J.CEP.2012.06.004.

[20] I. De Marco, O. Knauer, F. Cice, A. Braeuer, E. Reverchon, Interactions of phase equilibria, jet fluid dynamics and mass transfer during supercritical antisolvent micronization: the influence of solvents, Chem. Eng. J. 203 (2012) 71–80, https://doi.org/10.1016/J.CEJ.2012.06.129.

[21] J.O. Werling, P.G. Debenedetti, Numerical modeling of mass transfer in the supercritical antisolvent process: miscible conditions, J. Supercrit. Fluids 18 (2000) 11–24, https://doi.org/10.1016/S0896-8446(00)00054-1.

[22] E. Reverchon, R. Adami, G. Caputo, I. De Marco, Spherical microparticles production by supercritical antisolvent precipitation: interpretation of results, J. Supercrit. Fluids 47 (2008) 70–84, https://doi.org/10.1016/J.SUPFLU.2008.06.002.

[23] I. De Marco, E. Reverchon, Influence of pressure, temperature and concentration on the mechanisms of particle precipitation in supercritical antisolvent micronization, J. Supercrit. Fluids 58 (2011) 295–302, https://doi.org/10.1016/J.SUPFLU.2011.06.005.

[24] A. Gokhale, B. Khusid, R.N. Dave, R. Pfeffer, Effect of solvent strength and operating pressure on the formation of submicrometer polymer particles in supercritical microjets, J. Supercrit. Fluids 43 (2007) 341–356, https://doi.org/10.1016/J.SUPFLU.2007.05.012.

[25] E. Reverchon, E. Torino, S. Dowy, A. Braeuer, A. Leipertz, Interactions of phase equilibria, jet fluid dynamics and mass transfer during supercritical antisolvent micronization, Chem. Eng. J. 156 (2010) 446–458, https://doi.org/10.1016/J.CEJ.2009.10.052.

[26] E. Badens, O. Boutin, G. Charbit, Laminar jet dispersion and jet atomization in pressurized carbon dioxide, J. Supercrit. Fluids 36 (2005) 81–90, https://doi.org/10.1016/J.SUPFLU.2005.03.007.

[27] S. Dowy, A. Braeuer, R. Schatz, E. Schluecker, A. Leipertz, CO_2 partial density distribution during high-pressure mixing with ethanol in the supercritical antisolvent process, J. Supercrit. Fluids 48 (2009) 195–202, https://doi.org/10.1016/J.SUPFLU.2008.10.017.

[28] J.O. Werling, P.G. Debenedetti, Numerical modeling of mass transfer in the supercritical antisolvent process, J. Supercrit. Fluids 16 (1999) 167–181, https://doi.org/10.1016/S0896-8446(99)00027-3.

[29] M. Mukhopadhyay, S. Singh, Refining of crude lecithin using dense carbon dioxide as anti-solvent, J. Supercrit. Fluids 30 (2004) 201–211, https://doi.org/10.1016/j.supflu.2003.08.001.

[30] A. Martín, M.J. Cocero, Numerical modeling of jet hydrodynamics, mass transfer, and crystallization kinetics in the supercritical antisolvent (SAS) process, J. Supercrit. Fluids 32 (2004) 203–219, https://doi.org/10.1016/J.SUPFLU.2004.02.009.

[31] Y.P. de Diego, H.C. Pellikaan, F.E. Wubbolts, G.J. Witkamp, P.J. Jansens, Operating regimes and mechanism of particle formation during the precipitation of polymers using the PCA process, J. Supercrit. Fluids 35 (2005) 147–156, https://doi.org/10.1016/J.SUPFLU.2004.12.012.

[32] A. Martín, M.J. Cocero, Micronization processes with supercritical fluids: fundamentals and mechanisms, Adv. Drug Deliv. Rev. 60 (2008) 339–350, https://doi.org/10.1016/J.ADDR.2007.06.019.

[33] P. Imsanguan, S. Pongamphai, S. Douglas, W. Teppaitoon, P.L. Douglas, Supercritical antisolvent precipitation of andrographolide from Andrographis paniculata extracts: effect of pressure, temperature and CO_2 flow rate, Powder Technol. 200 (2010) 246–253, https://doi.org/10.1016/J.POWTEC.2010.02.031.

[34] A. Montes, L. Wehner, C. Pereyra, E.J. Martínez de la Ossa, Generation of microparticles of ellagic acid by supercritical antisolvent process, J. Supercrit. Fluids 116 (2016) 101–110, https://doi.org/10.1016/J.SUPFLU.2016.05.019.

[35] F. Mattea, Á. Martín, A. Matías-Gago, M.J. Cocero, Supercritical antisolvent precipitation from an emulsion: -carotene nanoparticle formation, J. Supercrit. Fluids 51 (2009) 238–247, https://doi.org/10.1016/j.supflu.2009.08.013.

[36] R.L. Matos, T. Lu, V. Prosapio, C. McConville, G. Leeke, A. Ingram, Coprecipitation of curcumin/PVP with enhanced dissolution properties by the supercritical antisolvent process, J. CO2 Util. 30 (2019) 48–62, https://doi.org/10.1016/J.JCOU.2019.01.005.

[37] P. Franco, E. Reverchon, I. De Marco, Zein/diclofenac sodium coprecipitation at micrometric and nanometric range by supercritical antisolvent processing, J. CO2 Util. 27 (2018) 366–373, https://doi.org/10.1016/J.JCOU.2018.08.015.

[38] M.C. Guamán-Balcázar, A. Montes, C. Pereyra, E.M. de la Ossa, Precipitation of mango leaves antioxidants by supercritical antisolvent process, J. Supercrit. Fluids 128 (2017) 218–226, https://doi.org/10.1016/J.SUPFLU.2017.05.031.

[39] E. Widjojokusumo, B. Veriansyah, R.R. Tjandrawinata, Supercritical anti-solvent (SAS) micronization of Manilkara kauki bioactive fraction (DLBS2347), J. CO2 Util. 3–4 (2013) 30–36, https://doi.org/10.1016/J.JCOU.2013.09.001.

[40] D. Villanueva Bermejo, E. Ibáñez, G. Reglero, C. Turner, T. Fornari, I. Rodriguez-Meizoso, High catechins/low caffeine powder from green tea leaves by pressurized liquid extraction and supercritical antisolvent precipitation, Sep. Purif. Technol. 148 (2015) 49–56, https://doi.org/10.1016/j.seppur.2015.04.037.

[41] A. Visentín, M. Cismondi, D. Maestri, Supercritical CO 2 fractionation of rosemary ethanolic oleoresins as a method to improve carnosic acid recovery, Innov. Food Sci. Emerg. Technol. 12 (2011) 142–145, https://doi.org/10.1016/j.ifset.2011.01.004.

[42] A. Sánchez-Camargo, J. Mendiola, A. Valdés, M. Castro-Puyana, V. García-Cã nas, A. Cifuentes, M. Herrero, E. Ib nez, Supercritical antisolvent fractionation of rosemary extracts obtained by pressurized liquid extraction to enhance their antiproliferative activity, J. Supercrit. Fluids 107 (2016) 581–589, https://doi.org/10.1016/j.supflu.2015.07.019.

[43] S.N. Joung, C.W. Yoo, H.Y. Shin, S.Y. Kim, K.-P. Yoo, C.S. Lee, W.S. Huh, Measurements and correlation of high-pressure VLE of binary CO2–alcohol systems (methanol, ethanol, 2-methoxyethanol and 2-ethoxyethanol), Fluid Phase Equilib. 185 (2001) 219–230, https://doi.org/10.1016/S0378-3812(01)00472-1.

[44] C.J. Chang, C.-Y. Day, C.-M. Ko, K.-L. Chiu, Densities and P-x-y diagrams for carbon dioxide dissolution in methanol, ethanol, and acetone mixtures, Fluid Phase Equilib. 131 (1997) 243–258, https://doi.org/10.1016/S0378-3812(96)03208-6.

[45] Ž. Knez, M. Škerget, L. Ilič, C. Lütge, Vapor–liquid equilibrium of binary CO2–organic solvent systems (ethanol, tetrahydrofuran, ortho-xylene, meta-xylene, para-xylene), J. Supercrit. Fluids 43 (2008) 383–389, https://doi.org/10.1016/J.SUPFLU.2007.07.020.

[46] V.L. Singleton, R. Orthofer, R.M. Lamuela-Ravents, Analysis of total phenols and other oxidations substrates and antioxidants by means of Folin–Ciocalteu reagent, Polyphenols Flavonoids 25 (1974) 152–178.

[47] W. Brand-Williams, M.E. Cuvelier, C. Berset, Use of a free radical method to evaluate antioxidant activity, LWT - Food Sci. Technol. 28 (1995) 25–30.

[48] G. Vicente, M.R. García-Risco, T. Fornari, G. Reglero, Isolation of carsonic acid from rosemary extracts using semi-preparative supercritical fluid chromatography, J. Chromatogr. A 1286 (2013) 208–215, https://doi.org/10.1016/j.chroma.2013.02.044.

[49] E. Reverchon, I. De Marco, Mechanisms controlling supercritical antisolvent precipitate morphology, Chem. Eng. J. 169 (2011) 358–370, https://doi.org/10.1016/J.CEJ.2011.02.064.

[50] Z. Sroka, W. Cisowski, Hydrogen peroxide scavenging, antioxidant and anti-radical activity of some phenolic acids, Food Chem. Toxicol. 41 (2003) 753–758, https://doi.org/10.1016/S0278-6915(02)00329-0.

[51] J. Dai, R.J. Mumper, J. Dai, R.J. Mumper, Plant phenolics: extraction, analysis and their antioxidant and anticancer properties, Molecules 15 (2010) 7313–7352,

https://doi.org/10.3390/molecules15107313.
[52] N. Martins, L. Barros, I.C.F.R. Ferreira, In vivo antioxidant activity of phenolic compounds: facts and gaps, Trends Food Sci. Technol. 48 (2016) 1–12, https://doi.org/10.1016/J.TIFS.2015.11.008.
[53] K. Rìznar, S. Celan, M. Skerget, Z. Knez, Solubility of carnosic acid and carnosol from rosemary extract in supercritical CO_2, Acta Chum. Slov. 55 (2008) 516–520.
[54] A. Cháfer, T. Fornari, A. Berna, E. Ibañez, G. Reglero, Solubility of solid carnosic acid in supercritical CO2 with ethanol as a co-solvent, J. Supercrit. Fluids 34 (2005) 323–329, https://doi.org/10.1016/J.SUPFLU.2004.10.009.
[55] D. Villanueva-Bermejo, F. Zahran, D. Troconis, M. Villalva, G. Reglero, T. Fornari, Selective precipitation of phenolic compounds from Achillea millefolium L. extracts by supercritical anti-solvent technique, J. Supercrit. Fluids 120 (2017) 52–58, https://doi.org/10.1016/j.supflu.2016.10.011.